The Selective Hydrogenation of Furfural over Supported Palladium Nanoparticle Catalysts Prepared by Sol-Immobilisation: Effect of Catalyst support and Reaction Conditions

Reem Albilali,[*1] Mark Douthwaite,[2] Qian He[2] and Stuart H. Taylor*[2]

[1] *Department of Chemistry, College of Science, Imam Abdulrahman Bin Faisal University, P.O. Box 1982, Dammam 31441, Saudi Arabia.*

[2] *Cardiff Catalysis Institute, School of Chemistry, Cardiff University, Main Building, Park Place, Cardiff, CF10 3AT, United Kingdom.*

* Corresponding authors e-mail: taylorsh@cardiff.ac.uk, ralblali@iau.edu.sa

Abstract

The selective hydrogenation of bio-derived furfural was investigated under mild conditions using a series of supported palladium catalysts prepared by a sol-immobilisation technique. Catalysts using alumina and titania supports were more selective towards tetrahydrofurfural alcohol. The catalytic activity of 1.19 % Pd/TiO_2 was evaluated under different reaction conditions and higher selectivity towards tetrahydrofurfural alcohol was observed when using 2-propanol as a solvent, and the yield of tetrahydrofurfural alcohol decreased as reaction temperature increased. The performance of the Pd catalyst was enhanced by the addition of Pt and a 95 % yield of tetrahydrofurfural alcohol was achieved. Catalysts were characterised by a range of techniques, and the synergistic effect of adding Pt to Pd was due to an electronic promotional effect.

Keywords: Hydrogenation, furfural, heterogeneous catalysis, biomass, tetrahydrofurfuryl alcohol

1. Introduction

The social, political and environmental issues surrounding the manufacture of 1st generation biofuels has limited their global application somewhat.[1] As a consequence, is that interest in the synthesis of liquid fuels and fine-chemicals from lignocellulosic feedstocks has increased, due to its large natural abundance and sustainability.[2, 3] However, the valorisation of such feedstocks are currently economically limited due to the extensive processing steps required. As such, interest in the development of technologies to facilitate the conversion of lignocellulosic feedstocks to high-value compounds has increased significantly in recent years.[4] Furfural (FF) is produced from the hydrolysis and dehydration of lignocellulosic feedstocks.[2] It has very few direct applications, but is considered to harbour a lot of potential as a highly desirable platform chemical.[5]

The selective hydrogenation of FF over heterogeneous catalysts has been investigated in significant detail in recent years, the progress of which has been documented in some current reviews.[6, 7] The products of this hydrogenation reaction have a variety of different industrial applications. Furfuryl alcohol (FA), which is produced from the chemoselective hydrogenation of the formyl group, is used as a monomer for the formation of furanic resins,[8] in addition to it's potential as a fuel.[9] Furthermore, the total hydrogenation of FF gives tetrahydrofurfuryl alcohol (THFA), which is considered to be an environmentally benign green solvent due to its biodegradable nature[10]. The hydrodeoxygenation of FF produces 2-methylfuran (MF), which also has potential to be utilised as a fuel additive.[11] In addition to the above, the hydrogenation of FF can also lead to the formation of numerous other products via ring-opening, decarbonylation and rearrangement pathways.[12] Accordingly, tuning the reaction selectivity towards a specific product is challenging but can be achieved through catalyst design.

It is clear from studies of FF hydrogenation that the selection of catalytic metal, support, reaction conditions and solvent choice can drastically influence the product distribution. Polar

solvents have been found to significantly promote the rate of these hydrogenation reactions, but can also lead to the formation of acetyl and/or ester adducts.[13] It has been shown that the formation of these by-products can be suppressed through the utilization of some non-polar solvents, but solvents of this nature also significantly reduce the reaction rate. Further drastic changes in the selectivity profile can also be observed; water facilitates the re-arrangement of FF to cyclopentanone[14, 15] and the ring opening of furfuryl alcohol (FA) to produce diols.[16] Dichloroethane was found to promote the hydrodeoxygenation (HDO) of FF to methyl furan (MF).[17]

The hydrogen pressure in the system can also significantly affect the product distribution. LuO *et al.*[18] showed recently that increasing the hydrogen pressures in the presence of a 10 % Pt/C catalyst increased selectivity to furfuryl alcohol, and that low pressures favoured hydrogenolysis reactions to produce furan. This is consistent with a previous DFT study by Vlachos and co-workers[19] who showed that the product distribution is typically dependent on the energy and conformation of adsorbed FF, which in turn is driven by the concentration of hydrogen adsorbed to the surface.

Additional work has investigated the effect of different support and metal combinations. A study by Sitthisa *et al.*[20] showed that Cu, Pd and Ni supported independently on SiO_2, each favoured different reaction pathways for the hydrogenation of FF in a continuous flow system. A considerable number of recent studies have focussed on developing supported metal catalysts with mono and bimetallic combinations of transition metals, and through optimisation of the materials and reaction conditions, extremely high yields of FA are obtainable.[21-24] Particle size effects are also known to have a profound effect on chemoselectivity, with an example being the hydrogenation of α,β-unsaturated aldehydes,[25-27] an effect which is likely to be due to an alteration of the substrates mode of adsorption.[28]

Whilst a substantial amount of literature reports highly effective systems for the selective hydrogenation and transfer hydrogenation of FF to FA, a much smaller quantity of publications focus on the total hydrogenation of FF to THFA. Table 1 contains some catalytic systems which are reported for the total hydrogenation of FF to FA.

Although there are numerous examples of catalytic systems which report exceptionally high yields to THFA from FF, in most cases either a high reaction temperature, high H_2 pressure or both are required to achieve them. As such, it would clearly be advantageous to develop a system which could produce similar yields of THFA but under milder reaction conditions.

The preparation of supported metal catalysts by the sol-immobilisation method can have a dramatic effect on the physicochemical properties of the supported metal nanoparticles.[37] This technique utilizes a stabilising agent such as polyvinyl alcohol (PVA) or polyvinyl pyrolidone (PVP) to control the growth of the nanoparticles and subsequently leads to the formation of colloidal metal nanoparticles of a well-defined particle size.[38] Once the colloids are formed, the metal is subsequently reduced, typically using a reducing agent such as $NaBH_4$. The support material is subsequently added and the pH of the solution is often adjusted to ensure full immobilisation of the metal. The adsorption of the stabilised nanoparticles are typically dependent on the nature of the stabiliser and the isoelectric point, surface functionality and surface area of the support.[39, 40] It is the defined and often tuneable metal particle sizes that make this technique so desirable.

To the best of our knowledge, studies investigating the activity of supported metal catalysts prepared *via* sol-immobilization method for the liquid phase hydrogenation of FF are limited. Only a study conducted by Rogers *et al.*[34] highlighted the potential of using Pd/TiO_2 catalysts prepared by a sol-immobilization method for the selective hydrogenation of FF, determining that the size of the Pd nanoclusters and the nature of the reaction sites have a significant

influence on the reaction selectivity. In this study, we investigate the effect of reaction conditions and support materials on the performance of supported Pd nanoparticles for the selective hydrogenation of FF. All the catalysts were prepared by the sol-immobilisation method to produce catalysts with small and narrow particle size distributions and tested under very mild conditions for the liquid phase hydrogenation of FF. We also present results showing how the catalytic performance of Pd nanoparticles can be enhanced by the addition of Pt to produce supported bimetallic catalysts.

2. Experimental

2.1 Materials (Source and Purity)

Potassium tetrachloropalladate(II) (99.99 %, Alfa Aesar), sodium borohydride (98 %, Sigma-Aldrich) polyvinyl alcohol (99 %, Sigma-Aldrich), furfuryl alcohol (98 %, Sigma-Aldrich), furfural (99 %, Sigma-Aldrich), γ-valerolactone (99 %, Sigma-Aldrich), magnesium oxide (99.9 %, BDH) and iron (II, III) oxide (99.99 %, Sigma-Aldrich), titania P.25 (99.9 %, Degussa), activated charcoal (DARCO G-60, ACROS). All experiments were carried out using 2-propanol (99.5 %, Fisher Scientific) as a solvent, unless otherwise stated.

2.2 Catalyst Preparation

The experimental method for the preparation of the mono- and bimetallic catalysts by sol-immobilisation is as follows: Desired quantities of K_2PdCl_4 (0.0183 mol) and/or H_2PtCl_6 (0.0184 mol) was added to H_2O (800 mL g^{-1} of catalyst prepared) and stirred. To this solution, polyvinyl alcohol (metal/PVA = 0.65 weight ratio, weight average molecular weight Mw ¼ 9000–10 000 g mol^{-1}, 80 % hydrolysed) was added. Subsequently, $NaBH_4$ ($NaBH_4$/metal (mol/mol) = 5) was then introduced. After 30 minutes of sol generation, the colloid was immobilised by adding support (0.99 g) and the solution was acidified to pH 2 (0.1 M, H_2SO_4)

under vigorous stirring. After 1 hour, the slurry was filtered, the catalyst washed thoroughly with distilled water, and dried at 110 ºC for 16 h.

The experimental method for the preparation of the monometallic Pd/TiO_2 catalyst by an impregnation method is as follows: K_2PdCl_4 (0.00915 mol) was dissolved in 1.6 mL of deionised water and stirred slowly at 80 ºC until the salt dissolved completely. The support (0.495 g, TiO_2 commercial P25) was subsequently added to the solution under vigorous stirring at 80 ºC until a thick paste was formed. The paste was dried at 110 ºC for 16 h and the subsequent material was finely ground and calcined at 400 ºC under static air for 3 hours with a ramp rate of 20 ºC min^{-1}.

2.3 Catalyst Testing

Furfural hydrogenation was performed between 30 °C and 60 °C in a Colaver glass reactor. The reactor was charged with FF solution (15 mL; 0.3 M in 2-propanol) and the desired amount of catalyst, typically FF/metal molar ratio = 500, was added to the solution. The reactor was sealed, and purged three times with H_2 (3 bar) whilst stirring (800 rpm), before finally being charged with H_2 (1-3 bar). A continuous reaction pressure was maintained throughout the reaction in order to replenish any H_2 consumed. The reaction was conducted for 120 minutes, unless otherwise stated.

Catalyst reusability was investigated after the hydrogenation reaction of FF, the catalyst was separated using a simple filtration method and washed with 50 mL of solvent 2-propanol. The separated catalyst was dried at room temperature for 24 hours before being reused. The recycling experiments were continued using the same catalyst and same experimental protocol for five cycles.

2.4 Quantification of Products

The reaction effluent was analysed by GC (Agilent 7890B) fixed with a CP-Wax 52 CB column (25 m x 0.53 mm x 2.0 µm) and a FID. n-Octane was used as an external standard for product quantification. A combination of GC and GC-MS was used to determine the chemical identity of the products, and comparison with authentic standards was carried out to ensure correct identification. The reactant conversion, products selectivity and product yield were calculated on mole basis using the following formulae:

% Conversion of (FF) = [(Initial moles of FF - Final moles of FF) / Initial mole of FF)] x 100

% Selectivity = (Moles of product formed / (Total moles of products identified) x 100

% Yield = [Moles of product formed / Moles of $FF_{(Start)}$] x 100

Attempts were made to calculate the Pd dispersion of the catalysts and determine the initial rate of each catalyst directly from the number of Pd sites detected by CO chemisorption. However, it has been reported previously that the presence of a stabiliser can significantly reduce the quantity of CO that can adsorb to the surface of catalysts prepared by the sol-immobilisation method.[41] As such, in this study, the initial rate measurements were estimated by dividing the moles of substrate converted by the mass of metal in the reaction per unit time (h) after 30 minutes.

2.5 Catalyst Characterisation

Powder X-ray diffraction (XRD) patterns were collected using a PANalytical X'pert Pro diffractometer with a Ni-filtered CuK_{α} radiation source operating at 40 kV and 40 mA. The

diffraction patterns were recorded over the 2θ range 10 – 80º, and phases identified by matching to entries in the International Centre for Diffraction Data (ICDD) database.

X-ray photoelectron spectra (XPS) were recorded on a Kratos Axis Ultra DLD spectrometer using a monochromatic Al Kα X-ray source (100 W). Spectra were recorded at analyser pass energies of either 160 eV (survey scans) or 40 eV (detailed scans). Binding energies were referenced to the C(1s) binding energy of adventitious carbon contamination at 284.7 eV, and data were quantified using CasaXPSTM v2.3.15 software, using sensitivity factors supplied by the manufacturer.

Transmission electron microscopy (TEM) was carried out using a JEOL JEM-2100 with a LaB6 filament operating at 200 kV. Powdered catalyst samples were dry dispersed onto lacey carbon-coated 400 mesh copper grids. The mean particle size distributions (based on 300 particles) were subsequently measured using Image J software.

Scanning Transmission electron microscopy (STEM) was carried out using an aberration corrected JEOL JEM ARM 200CF microscope operating at 200kV. Powdered catalyst samples were dry dispersed onto lacey carbon-coated 300 mesh copper grids. X-ray energy dispersive (XEDS) spectra were acquired from individual metal nanoparticles by rastering the beam over the entire metal particle, while using a JEOL Centurio 0.9sr silicon drift detector.

Scanning electron microscopy (SEM) was conducted on a Hitachi TM3030PLUS microscope equipped with a Quantax70 energy-dispersive X-ray spectroscope (EDX, Microanalysis System, Oxford Instruments).

Microwave plasma-atomic emission spectroscopy (MP-AES) was carried out using an Agilent 4100 instrument to determine the metal loading. A known mass of catalyst was added to a dilute aqua regia solution (50 mL of 10 % aqueous solution) and left to digest for 16 h. The digested solution was subsequently filtered using PTFE filters (Acrodisc PVDF 0.45 μl) to eradicate any remaining residual support material from the solution. Samples were

introduced into a stream of nitrogen plasma *via* a single pass spray chamber at a pressure of 120 kPa in the absence of any air injection. The instrument was calibrated with 2.5 ppm, 5 ppm and 10 ppm solutions of the metal which were prepared from analytical standard solutions (Agilent, 1000 ppm). Samples were tested three times, and an average of the three results used to calculate elemental compositions.

Inductively Coupled Plasma-mass spectrometry (ICP-MS) analysis was performed in order to quantify any metal leaching during the test reactions to determine catalyst performance. The analysis was performed using an Agilent ICP-MS 7900 instrument. Quantitative analysis of the post-reaction effluents were performed in duplicate, and metal concentration determined following calibration with certified standards.

3. Results and Discussion

3.1 Effect of the support on catalytic performance and reaction mechanism

In order to expand on the recent work by Rogers *et al.*,[34] a series of monometallic Pd catalysts were prepared using a similar colloidal method. Different support materials were utilised in order to investigate how the support affects the activity and selectivity of the Pd nanoparticles. Each reaction was conducted under mild conditions (3 bar hydrogen, 30 °C) in 2-propanol solvent. The results from the initial catalytic screening experiments are displayed in Table 2. The products expected from the hydrogenation of FF using these catalysts are presented in Figure 1.

It is evident that all the catalysts are active for this reaction and that the support material significantly influences the performance of Pd nanoparticles. The Pd supported on TiO_2, C, MgO and Al_2O_3 achieved full conversion after 180 min, while only 64.2 % conversion was observed with Pd/Fe_3O_4. The initial rates revealed that the Pd/C catalyst exhibited the highest activity of the catalysts tested. An initial rate of 5.21mol g^{-1} h^{-1} was calculated for this catalyst,

which was approximately 85 % greater than the initial rate observed for Pd supported on TiO_2, MgO and Al_2O_3. Despite the high activity associated with the Pd/C catalyst, the observed product distribution was undesirable, as many unknown products were formed. Previous work has shown that some catalytic systems lead to the formation of ring opening products such as 1,2-pentandiol.[16] The formation of many of these ring opening products can be discounted here, as none of them were observed in the post reaction effluent. Another potential explanation is the participation of the 2-propanol solvent in competitive reactions, leading to the formation of the corresponding ether or acetyl adduct. Merlo and co-workers[22] reported that the formation of the corresponding isopropanol ether is possible during the catalysed liquid phase hydrogenation of FF in the presence of 2-propanol, but we did not observe such products. Interestingly, the Pd/C appears to facilitate hydrogenolysis of FF to MF, and some of the unknown products may be either intermediates or additional products formed during this pathway. Nevertheless, the conclusion is that the Pd/C catalyst did not show the control over selectivity required.

The other supports tested were more selective to a smaller range of products, and they did not produce significant quantities of unknown products. The Al_2O_3 and TiO_2 supports led to the formation of γ-valerolactone (GVL). It is possible that Bronsted acidic sites in the catalyst are promoting the ring opening of FA to levulinic acid (LA), which can subsequently be reduced and cyclise to give GVL.

Interestingly, chemoselective hydrogenation is observed with the Fe_3O_4 and MgO based catalysts, as they appear to efficiently hydrogenate the unsaturated functional groups in the furan ring. Consequently, high quantities of tetrahydrofurfural (THFF) are observed in the reactions using these catalysts.

Comparison of selectivity at relatively low conversions for catalysts with different supports can also be made from the data in Table 2. For all catalysts, the selectivity after 30 minutes reaction time favours the formation of FA over all other products (THFA, 2MF, GVL, and THFF), suggesting that C=O hydrogenation is favoured over the hydrogenation of the unsaturated groups within the furan ring. As FA is consumed, an increase in the quantity of THFA in the system is observed. Whilst the majority of FA consumed between 30 and 120 minutes is likely to be a result of sequential hydrogenation to THFA, the increase in the yield of THFA does not account for all the FA consumed during this time. This suggests that there are additional competitive reaction pathways proceeding from FA. As discussed previously, Bronsted acidity can promote the formation of GVL from FA which may account for perhaps some of the GVL observed in the system. Another interesting observation that can be made is that THFF appears to be relatively stable in the system; only small quantities of THFF are consumed from 120 to 180 minutes. This implies that the C=O moiety in THFF is more difficult to hydrogenate than the furan ring in FA to form THFA. A possible explanation for this is that the C=O in THFF forms a hydrogen bond with the polar O-H moiety in the 2-propanol solvent, while the conjugated π-bond in the furan ring in FA cannot interact with the solvent in the same manor. It's possible that this solvent-substrate interaction would reduce the affinity of the C=O moiety to adsorb onto the surface of the catalyst which would ultimately reduce the rate of the C=O hydrogenation. Hu *et. al.*[42] observed a similar observation for the catalytic liquid phase hydrogenation of furfural in methyl formate. It was suggested that the high quantities of THFF observed in their system was a result of the ability of the C=O moiety in furfural to form hydrogen bonds with the methyl formate, ultimately making the carbonyl group more difficult to hydrogenate than the furan ring in furfural.

The comparison of the selectivity towards THFA (the desired product) at an initial time of 30 minutes shows that the Pd/TiO_2 catalyst has the higher selectivity towards THFA (20.2 %)

compared with 4.2 %, 2.3 %, 5.8 % and 13.3 % for Pd/C, Pd/MgO, Pd/Al_2O_3 and Pd/Fe_2O_3 respectively (Table 2). Furthermore, it is clear that the yield of THFA produced increases significantly with reaction time in the presence of Pd/TiO_2 and Pd/Al_2O_3. This increase in the yield of THFA is associated with a decrease in the selectivity towards FA. No FA was detected after 180 minutes of this reaction, in which the selectivity towards THFA reached a maximum of 42 % and 36.4 % with the Pd/TiO_2 and Pd/Al_2O_3 catalysts respectively. As such, we can conclude that FA is an intermediate in the conversion of FF to THFA. Furthermore, the yield of THFA is influenced by the type of support used. Figure 2 shows that the maximum yield of 42 % was observed for Pd/TiO_2. Given that THFA is the desired product in this study, further reaction optimisation and investigation was focussed on the Pd/TiO_2 catalyst.

The powder X-ray diffraction patterns for catalysts on different supports are displayed in Figure S1. The data implies that the Pd metal is well dispersed on all supports, as no diffraction from Pd phases is observable. MP-AES was used to determine the Pd metal loadings associated with each of the catalysts, the results of which are shown in Table 2 and indicate that significant loadings of Pd are present. The range of the Pd loading on different supports varied slightly, but in each case the Pd metal loading fell within the range 1.19 to 1.57 wt.%. Thus, we can conclude that the successful immobilisation of Pd onto each support material was achieved.

In order to determine whether reducing the metal loading influences the activity of the Pd nanoparticles, an additional Pd/TiO_2 catalyst was prepared with a lower Pd loading and was subsequently tested under the same reaction conditions. The comparison of these two Pd/TiO_2 catalysts is displayed in Table S1. MP-AES confirmed that an appropriate reduction in the Pd loading was achieved as the Pd loading in this catalyst was measured to be 0.57 %. Transmission electron microscopy (TEM) was subsequently utilised to assess whether reducing the metal loading has an influence on the Pd particle size distribution. TEM images and corresponding particle size distributions of the two Pd/TiO_2 catalysts with different Pd

loadings are displayed in Figure 3. It can be noted that the palladium particles were well dispersed on the titania support for both catalysts. A small decrease in the mean particle size was observed when decreasing the palladium loading, as the mean particle size reported for the 1.19 % Pd/TiO_2 and 0.57 % Pd/TiO_2 catalysts was 3.32 nm and 2.97 nm respectively. The evaluation of catalytic performance for these catalysts (Table S1) reveals that the conversion after 30 min decrease from 36.4 % to 28.2 % when the Pd loading was reduced from 1.19 % to 0.57 %. This decrease in conversion corresponds to a 15 % decrease in the initial reaction rate, decreasing from 2.75 to 2.32 mol g^{-1} h^{-1}. Assessment of the corresponding product distributions after 30 minutes (conversions of 28.2 % and 36.4 %) shows that there was no significant change in the quantity of FA observed, with values of 38.4 % and 41.9 % for the reaction catalysed by the 0.57 % Pd/TiO_2 and 1.19 % Pd/TiO_2 respectively. In contrast, the yield of THFA decreases significantly from 20 % to 11 % when reducing the Pd loading from 1.19 % to 0.57 %. This decrease in the yield of THFA observed upon reducing the Pd loading is associated with a 17 % increase in the yield of THFF observed, as the selectivity increased from 23.6 % to 40.7 % when the Pd loading was reduced. This is consistent with a previous observation, that the hydrogenation of the C=O species may be more difficult when the furan ring is saturated, accordingly, the catalyst with low metal loading shows higher quantities of THFF. Increasing the metal loading can enhance the hydrogenation of C=O over Pd nanoparticles, which is more difficult to hydrogenate using the 0.57 % Pd/TiO_2, resulting in more selectivity towards THFA at higher Pd loading.

Figure 4 shows the yield of THFA and FA produced after a reaction time of 120 minutes. In the presence of the 1.19 % Pd/TiO_2, no FA was observed and the yield of THFA reached 43 %, while only 20 % yield of THFA was observed for the 0.57 % Pd/TiO_2 catalyst with a substantial quantity of FA still present in the post reaction effluent (12%). These results reveal

that the rate of sequential hydrogenation of FA to THFA decreases by reducing the Pd loading, which is consistent with the decrease of the initial rate of overall hydrogenation.

There are numerous examples of similar catalytic systems which facilitate the transfer hydrogenation of furfural in the presence of 2-propanol.[43-46] In each of these examples however, significantly higher reaction temperatures (110 to 200 ºC) were required in order to facilitate the transfer hydrogenation. Nevertheless, it was important to eradicate the possibility that these reactions were taking place within this catalytic system. For this, additional reactions were conducted under N_2 using the same reaction conditions and catalyst, the results of which are displayed in Table S2. In the absence of H_2, no furfural conversion was observed suggesting that the reductions taking place require H_2. Furthermore, no acetone was observed in the post reaction solutions for the reactions in the presence of both H_2 and N_2, providing further evidence that the isopropanol does not provide hydrogen in the reaction. An additional reaction was subsequently conducted under N_2 in the presence of the TiO_2 support material in order to eradicate any possibility that this material was facilitating a transfer hydrogenation reaction. As with the reaction conducted in the presence of Pd/TiO_2, no conversion of FF or production of acetone was observed.

SEM-EDX analysis was carried out to provide more information about the morphology of these two catalysts. The results of which are displayed in Figure S2. Both catalysts exhibit similar morphologies. The Pd loading calculated using EDX for the 0.57 % Pd/TiO_2 and 1.19 % Pd/TiO_2 are 0.59% and 1.10% respectively, which is consistent with the Pd loading reported from MP-AES. The metal elemental mapping images for both catalysts are shown in Figure S3. It can be noted that Pd was less densely distributed in 0.57 % Pd/TiO_2 compared with the 1.19 % catalyst, this is most likely expected, as there is only a slight change in Pd particle size, from 2.97 nm to 3.32 nm for 0.57 % Pd/TiO_2 and 1.19 Pd/TiO_2 respectively. As such, it can be concluded that the density of Pd in the catalyst is predominantly related to the Pd content.

Considering that the applied FF/Pd molar ratio of 500:1 remained equal during catalyst testing, and there is no significant change in the mean particle size obtained from TEM images for both catalysts, hence we can conclude that the main factor which enhances the catalytic activity in 1.19 % Pd/TiO_2 catalyst is having a greater number of surface Pd sites available.

X-ray photoelectron spectroscopy (XPS) was conducted to obtain further information regarding the oxidation state of Pd and elemental distribution on the surface of each TiO_2 supported catalyst. The corresponding spectroscopic data is presented in Figure 5 and Table S3. Two dominant peaks with binding energies of 335.3 and 336.6 eV are observed in the spectra of each catalyst, and correspond to the Pd($3d_{5/2}$) spin-orbit coupled peaks of palladium. It is clear that Pd is present in both its metallic state (Pd^0) and oxidised state (Pd^{2+}) in all the catalyst samples. As shown in Figure 5, the Pd($3d_{5/2}$) peak can be fitted to two dominant peaks, with binding energies of 335.3 and 336.6 eV. The peak at 335.3 eV can be assigned to the metallic state of palladium, while the other peak at 336.6 eV can be assigned to Pd^{2+} in PdO.[47, 48] The Pd^0/Pd^{2+} ratio does not appear to correlate with differences in catalyst performance. The XPS spectrum for the used 1.19 % Pd/TiO_2 displayed in Figure 6 shows that only Pd^0 is present in the used catalyst, which indicates that PdO supported on TiO_2 readily reduces in the presence of H_2 at ambient temperature.[49]

To evaluate the leaching of Pd from each catalyst prepared using different supports, ICP-MS analysis was conducted on the post reaction effluent of each reaction (Table S4). Pd metal was detected in the post reaction effluents with each of the catalysts, but the concentration of Pd was low. In each case, less than 0.1 % of Pd was leached from each of the catalysts, which indicates that the binding of the metal nanoparticles to the different surfaces was a stable process under our reaction conditions.

As the 1.19 % Pd/TiO_2 catalyst was found to provide the highest yields of THFA, an additional investigation was conducted in order to enphasise the benefit of using the sol-immobilisation as a means of preparing the Pd supported catalysts. For this, an additional Pd/TiO_2 catalyst (Pd loading calculated to be 1.10 wt.%) was prepared using a conventional impregnation method and tested for the hydrogenation of furfural under the same reaction conditions. This results are displayed in Figure S4. It was determined that the catalyst prepared by the sol-immobilisation method displayed an initial activity approximately 80 % higher than the catalyst prepared by the conventional impregnation method. Interestingly, an 18 % reduction in selectivity to THFA was also observed with the catalyst prepared by the impregnation method. It is known that the sol-immobilisation method typically yields supported metal catalysts with a significantly smaller metal particle size with a narrower particle size distribution than identical catalysts prepared by impregnation methods.[50, 51] As such, the significant difference in the activity of these catalysts can be attributed to a particle size effect.

In order to evaluate the stability of the 1.19 % Pd/TiO_2 catalyst prepared by the sol-immobilisation method, a series of recycling experiments were conducted. The results from this study are displayed in Figure 7 and Table S5. The catalyst preserved catalytic activity for 2 cycles, as the initial rate of 2.74 mol g^{-1} h^{-1} remained constant during the first two runs. A slight decrease in the yield of THFA was observed in the second cycle, as the yield of THFA decrease from 43 % to 36 %. This decrease in the THFA is associated with a 14 % increase in the yield of FA, which indicates that the rate of the sequential hydrogenation of FA to THFA in the second run was reduced. In the third cycle, the catalytic activity in terms of initial rate decreased by 20 % from its original value with a 56 % decrease in the yield of THFA compared with the THFA yield from the first cycle. A further drop in the activity was observed during the fourth and fifth run, as the initial rate decreased by approximately 70 % with values of to 0.88 and 0.81 mol g^{-1} h^{-1} for the fourth and fifth cycles respectively, with a continuous decrease

in the yield of THFA observed upon subsequent reactions. This decrease in activity may be attributed to a number of possibilities, including leaching of Pd, a change of Pd particle size, and deactivation of some active sites on the surface of the catalyst. Leaching of Pd seems unlikely considering the low Pd leaching measured previously. Nevertheless, Pd leaching was measured after each run. The concentration of Pd in solution after each use was negligible, and was found to lie in the range 0.048 – 0.066 ppm. This corresponds to a maximum leaching of 0.1 % of available Pd in each use, and hence loss of active metal through leaching was not considered to be an important factor in the loss of activity on reuse.

The particle size distribution obtained from TEM images for the used 1.19 % Pd/TiO_2 catalyst after five cycles of use is shown in Figure S5. There was a slight increase in the mean particle size, with a value of 3.82 nm for the catalyst after five cycles, compared to 3.32 nm for the fresh catalyst. The slight increase of particle size will result in some loss of metal surface area, however the more drastic decrease of activity is greater than would be expected for the minor loss of metal area. Hence, we conclude that the loss of activity also has a contribution attributed to the deactivation of some active sites on the surface of the catalyst. Roger *et al*.[34] concluded that deactivation of 1% Pd/TiO_2 prepared using sol-immobilization and used for the liquid phase hydrogenation of FF under mild conditions (5 bar hydrogen, 25°C) was due to the formation of palladium carbide, which affected hydrogen dissociation and influenced the adsorption of C=O and C=C functionalities.

3.2 Effect of reaction conditions on catalyst performance

The reaction solvent usually has an impact on the catalytic activity in a liquid-phase reaction. A comparison of 2-propanl, 2-butanol, toluene and 1,2 dichloroethene as solvents was conducted to investigate the influence on the catalytic performance for FF hydrogenation. The experiments were carried out using a 1.19 % Pd/TiO_2 catalyst under 3 bar H_2, FF/Pd molar ratio = 500 and a temperature of 30 °C. The results of which are represented in Figure 8. It can

be observed that variation of the solvent can influence both the product distribution and reaction rate. Among the solvents tested, 2-butanol was found to facilitate the highest rate of FF hydrogenation with a conversion of 49 % after 30 minutes, compared with 36 %, 32 % and 13 % when using 2-propanol, 1,2 dichloroethene and toluene respectively. Despite the high rate of FF hydrogenation observed with 2-butanol, the selectivity towards THFA and FA decreased by 40 % and 45 % respectively, when compared to the reaction conducted in 2-propanol. This decrease in the THFA and FA selectivities was associated with a 30 % increase in the selectivity towards THFF in the presence of 2-butanol, which indicates that the hydrogenation of unsaturated bonds within the furan ring is more favourable than the hydrogenation of C=O on FF in 2-butanol. In contrast, the conversion decreased significantly by 62 % when the reaction was conducted in toluene instead of 2-propanol. Hu *et.al.*[42] reported that a shielding effect resulting from an interaction between the conjugated π system in both furfural and toluene can be a factor which negatively affects the rate of hydrogenation of both the furan ring and carbonyl group in furfural when the reaction was conducted in toluene. An additional explanation was proposed by Merlo *et al.*[22] who also observed a significant reduction in catalytic activity when comparing the rate of reaction in polar and non-polar solvents. It was noted that a significant reduction in catalytic activity was observed for a supported Pd catalyst when the reaction was conducted in the presence of toluene instead of isopropanol, where the dielectric constant (ε) of each equal 2.0 and 18.3 respectively.

Interestingly, a significant change in the product distribution is observed when the reaction was conducted in 1,2-dichloroethane. Large quantities of 2-MF and much lower quantities of FA, THFA were formed, suggesting that 1,2-dichloroethane favours hydrodeoxygenation (HDO) of FF over hydrogenation. The promotional effect of 1,2-dichloroethane on the HDO of FF has already been reported for reactions conducted in the presence of Ru-Pd/TiO_2 bimetallic catalysts.[17, 52]

Further experiments were conducted in order to evaluate the influence of the reaction temperature on the product distribution. The experiments were carried out using 1.19 % Pd/TiO_2 catalysts (conditions: 3 bar H_2, solvent 2-propanol). The results from these experiments are displayed in Table 3. It is evident that the initial rate increases as the temperature increases. However, the final conversion after 120 minutes decreased as the temperature was raised from 50 to 60 ºC. This decrease in catalytic activity could be due to formation of additional products which inhibit the catalytic performance, indeed the higher temperature resulted in an increased amount of unknown products, which are most likely of the type discussed earlier. Examination of the corresponding product distributions supports this theory, as less THFA and THFF and more FA were observed as the reaction temperature was increased. If we assume that the majority of the THFA is produced by the sequential hydrogenation of FA and THFF, it is likely that this reduction in THFA selectivity is also a result of this product inhibition. Another possible cause for this drop in performance may be a result of the high temperatures facilitating the hydrogenolysis of FF. This would likely result in the presence of residual C_1 species on the surface of the catalyst and would supplement the work by Rogers *et al.*[34], who recently identified that the formation of a Pd-carbide species is responsible for catalyst deactivation, reducing the efficiency of FF adsorption on the surface of the Pd cluster.

The catalytic performance of 1.19 %Pd/TiO_2 was evaluated at varying H_2 pressure from 1 to 3 bar at 30 °C. The results are summarised in Table 4. It is evident that the hydrogen pressure has a significant impact on the catalytic activity as the initial rate decreases markedly when the H_2 pressure was reduced from 3 to 1 bar. This decrease in the catalytic activity was also accompanied with a decrease in the yield of THFA and FA observed. These results can be attributed to a decrease in the availability of hydrogen in the system, which is a result of a decrease in dissolved H_2 as the reaction pressure decreases. Interestingly, at 3 bar hydrogen,

we reached 100 % conversion of FF with 44 % selectivity to THFA after only 120 minutes reaction time. A significant increase in the yield of unknown products was also observed as the H_2 pressure was reduced, which could indicate the reaction pathways, which typically lead to the formation of these unknowns, compete with the hydrogenation reaction pathways. Given that previous work has shown that the hydrogenolysis of FF to furan typically increases at the expense of the hydrogenation products as the H_2 pressure decreases,[18, 19] it is possible that this undesirable reaction leads to the formation of some of the unknown products in the system. If this is to be the case, we must assume that any furan produced from the hydrogenolysis of FF subsequently partakes in another reaction, as no furan is observed in these reactions. Assuming that the Pd carbide formation is a result of the hydrogenolysis of FF as suggested previously, it can be postulated that the formation of this species may also contribute to the drop in catalytic activity observed at lower H_2 pressures.

3.3 Bimetallic Pd-Pt/TiO_2 catalyst

In some cases, the addition of a second metal or a promoter can improve the catalytic activity and/or the selectivity to the desired compound. Recent work has highlighted the potential of using supported PdPt bimetallic catalysts in hydrogenation reactions.[53] For this reason, an equimolar bimetallic 0.97 % PdPt/TiO_2 catalyst was prepared by the same preparation method and tested for the hydrogenation of FF under our standard conditions (3 bar H_2, 30 °C). The catalytic performance of synthesised bimetallic 0.97 % PdPt/TiO_2 was compared with the monometallic 1.19 .% Pd/TiO_2 and 1 % Pt/TiO_2 catalysts as shown in Table 5. The results reveal that the bimetallic 0.97 % PdPt/TiO_2 catalyst was far more active than both the 1.19 %

Pd/TiO_2 and 1 % Pt/TiO_2 monometallic catalysts, as the initial rate calculated after 30 minutes increased to 11.03 mol g^{-1} h^{-1} compared with 2.75 and 0.66 mol g^{-1} h^{-1} for 1.19 t% Pd/TiO_2 and 1 % Pt/TiO_2 respectively. Taking into account that the Pt/TiO_2 catalyst was significantly less active than the Pd/TiO_2 catalyst, it is clear that there is a synergistic interaction between the Pd and Pt in the system. Furthermore, the comparison of the product distribution after 240 min for the three catalysts (Figure 9) shows that a 95 % yield of THFA can be achieved when utilizing the bimetallic 0.97 % $PdPt/TiO_2$, while only 43 % and 0.3 % was achieved for the 1.19 % Pd/TiO_2 and 1 %Pt/TiO_2 respectively.

The initial activity of these catalysts is also reflected in the corresponding product distribution. The poorly active Pt/TiO_2 displayed exceptionally high selectivity to FA with only trace quantities of the sequential hydrogenation product (THFA) observed. Clearly, Pt favours the hydrogenation of the formyl species over the hydrogenation of the furan ring, as no THFF was observed in the presence of this monometallic catalyst. Furthermore, the selectivity to THFF observed with the bimetallic system is also significantly lower than that observed with the Pd/TiO_2. This may also suggests that the 0.97 % Pd-Pt/TiO_2 catalyst was able to hydrogenate the THFF to THFA more effectively, which resulted in an increase in the yield of THFA, reaching 95% after 240 minutes. Another possibility is that Pt in the bimetallic $PdPt/TiO_2$ catalyst affects the chemoselectivity of the catalyst and as a result, a larger quantity of FA is produced from FF. Considering the mild reaction conditions used in this system, the exceptionally high yield of THFA highlights the potential of using bimetallic $PdPt/TiO_2$ catalysts for the valorisation of FF.

In order to gain more insight into the structure-activity relationship for the bimetallic 0.97 % $PdPt/TiO_2$ catalyst, characterization by TEM and XPS was conducted. Figure 10 represents TEM images of the $PdPt/TiO_2$ catalyst and the corresponding particle size distribution. Interestingly, a mean particle size of 1.94 nm was observed for the 0.97 $PdPt/TiO_2$ catalyst,

which is notably smaller than 3.32 nm reported for the 1.19 % Pd/TiO_2 catalyst. As shown in Figure 11, the $PdPt/TiO_2$ catalyst was characterized by aberration corrected scanning transmission electron microscopy (AC-STEM). The nanoalloy formation between Pd and Pt within individual particles was confirmed using X-ray energy dispersive spectra obtained from individual particles. No segregation or core-shell formation was detected using Z-contrast high angle annular dark field (HAADF) imaging. The formation of random alloy Pd-Pt nanoalloys was consistent with our previous report.[54] Hence it can be inferred that the improved activity of the bimetallic catalyst is influenced by an increased dispersion of the active metal species, and a combination of electronic promotional effects, as there is a synergistic combination of Pd and Pt.

XPS was subsequently utilised in order to further assess the surface nature of the Pd-Pt nanoparticles and oxidation state of Pd and Pt in the catalyst. Figure 12 shows the XPS spectrum for the 0.97 % $Pd-Pt/TiO_2$ catalyst and confirms the existence of metallic Pd and metallic Pt on the surface layers. As shown in Figure 12, the Pd($3d_{5/2}$) peak can be fitted to a single peak, with a binding energy of 334.6 eV which can be assigned to the metallic state of palladium, whilst there was no evidence for a Pd^{2+} peak, which is expected at 336.9 eV. In addition, the Pt(4f) signal can be fitted to two peaks, at 70.6 eV and 73.95 eV. These two peaks are attributed to Pt^0 and Pt^{2+} species, respectively.[55, 56] The elemental composition obtained from the XPS data is shown in Table S6. The single metallic oxidation state of Pd in the bimetallic catalyst is in clear contrast to the combination of Pd^0 and Pd^{2+} in the monometallic TiO_2 supported catalyst, and indicates there is an electronic modification of the surface Pd through interaction with Pt. We believe that this interaction is important for promoting the activity of FF hydrogenation and indicates that the wealth of bimetallic nanoparticles available for catalyst preparation are now worthey of much further study.

Conclusions

In this study, we have highlighted the potential of using sol-immobilisation as a method of preparing supported Pd-based catalysts for the liquid phase hydrogenation of FF. We have determined that the support material, reaction conditions and solvent system can have a significant effect on both the activity and product selectivity of Pd nanoparticles. Of the supports tested, TiO_2 provided the highest selectivity to THFA. Further tests conducted with this catalyst revealed how vital the reaction conditions are to control the reaction selectivity. Subsequent testing conducted in the presence of a $PdPt/TiO_2$ catalyst revealed that a yield of THFA in excess of 95 % could be achieved. It was suggested that this increase in performance was a result of an electronic promotional effect from the synergistic combination of Pd and Pt.

Acknowledgements

We would like to thank Professor Christopher J. Kiely from Lehigh University and the Cardiff Catalysis Institute, Cardiff University, for kind support with the aberration corrected STEM characterization. AlBilali gratefully acknowledges Imam Abdulrahman Bin Faisal University for the financial support, and Cardiff Catalysis Institute, School of Chemistry, for access to the facilities. Authors would like to thank Dr Greg Shaw for useful discussion and experimental assistance, Dr Thomas Davies for TEM collection, and Dr David Morgan for collection of XPS data.

References

1. M. M. Gui, K. T. Lee and S. Bhatia, *Energy*, 2008, **33**, 1646-1653.
2. J. P. Lange, *Biofuel. Bioprod. Bior.*, 2007, **1**, 39-48.
3. G. Berndes and J. Hansson, *Energ. Policy*, 2007, 35, 5965-5979.

4. R. A. Sheldon, *Green Chem.*, 2014, **16**, 950-963.

5. J. P. Lange, E. van der Heide, J. van Buijtenen and R. Price, *Chemsuschem*, 2012, **5**, 150-166.

6. R. Mariscal, P. Maireles-Torres, M. Ojeda, I. Sadaba and M. L. Granados, *Energ. Environ. Sci.*, 2016, **9**, 1144-1189.

7. X. D. Li, P. Jia and T. F. Wang, *ACS Catal.*, 2016, **6**, 7621-7640.

8. M. Choura, N. M. Belgacem and A. Gandini, *Macromolecules*, 1996, **29**, 3839-3850.

9. S. G. Kulkarni and V. S. Bagalkote, *J. Energ. Mater.*, 2010, **28**, 173-188.

10. N. S. Biradar, A. M. Hengne, S. N. Birajdar, P. S. Niphadkar, P. N. Joshi and C. V. Rode, *ACS Sustain. Chem. Eng.*, 2014, **2**, 272-281.

11. S. Srivastava, G. C. Jadeja and J. Parikh, *J. Mol. Catal. A-Chem.*, 2017, **426**, 244-256.

12. M. G. Dohade and P. L. Dhepe, *Green Chem.*, 2017, **19**, 1144-1154.

13. A. O'Driscoll, J. J. Leahy and T. Curtin, *Catal. Today*, 2017, **279**, 194-201.

14. R. Q. Fang, H. L. Liu, R. Luque and Y. W. Li, *Green Chem.*, 2015, **17**, 4183-4188.

15. M. Hronec, K. Fulajtarova and T. Liptaj, *Appl. Catal. A-Gen.*, 2012, **437**, 104-111.

16. R. F. Ma, X. P. Wu, T. Tong, Z. J. Shao, Y. Q. Wang, X. H. Liu, Q. N. Xia and X. Q. Gong, *ACS Catal.*, 2017, **7**, 333-337.

17. S. Iqbal, X. Liu, O. F. Aldosari, P. J. Miedziak, J. K. Edwards, G. L. Brett, A. Akram, G. M. King, T. E. Davies, D. J. Morgan, D. K. Knight and G. J. Hutchings, *Catal. Sci. Technol.*, 2014, **4**, 2280-2286.

18. J. Luo, M. Monai, H. Yun, L. Arroyo-Ramirez, C. Wang, C. B. Murray, P. Fornasiero and R. J. Gorte, *Catal. Lett.*, 2016, **146**, 711-717.

19. S. G. Wang, V. Vorotnikov and D. G. Vlachos, *ACS Catal.*, 2015, **5**, 104-112.

20. S. Sitthisa and D. E. Resasco, *Catal. Lett.*, 2011, **141**, 784-791.

21. Q. Q. Yuan, D. M. Zhang, L. van Haandel, F. Y. Ye, T. Xue, E. J. M. Hensen and Y. J. Guan, *J. Mol. Catal. A-Chem.*, 2015, **406**, 58-64.

22. A. B. Merlo, V. Vetere, J. F. Ruggera and M. L. Casella, *Catal. Commun.*, 2009, **10**, 1665-1669.

23. K. Fulajtarova, T. Sotak, M. Hronec, I. Vavra, E. Dobrocka and M. Omastova, *Appl. Catal. A-Gen.*, 2015, **502**, 78-85.

24. S. B. Liu, Y. Amada, M. Tamura, Y. Nakagawa and K. Tomishige, *Green Chem.*, 2014, **16**, 617-626.

25. M. J. Taylor, L. J. Durndell, M. A. Isaacs, C. M. A. Parlett, K. Wilson, A. F. Lee and G. Kyriakou, *Appl. Catal. B-Environ.*, 2016, **180**, 580-585.

26. F. Jiang, J. Cai, B. Liu, Y. B. Xu and X. H. Liu, *RSC Adv.*, 2016, 6, 75541-75551.

27. S. Ganji, S. Mutyala, C. Krishna, P. Neeli, K. Seetha, R. Rao and D. R. Burri, *RSC Adv.*, 2013, **3**, 11533-11538.

28. P. Gallezot and D. Richard, *Catal. Rev.*, 1998, **40**, 81-126.

29. N. Merat, C. Godawa and A. Gaset, *J. Chem. Technol. Biot.*, 1990, **48**, 145-159.

30. Y. Nakagawa and K. Tomishige, *Catal. Commun.*, 2010, **12**, 154-156.

31. Rodiansono, S. Khairi, T. Hara, N. Ichikuni and S. Shimazu, *Catal. Sci. Technol.*, 2012, **2**, 2139-2145.

32. Y. Nakagawa, K. Takada, M. Tamura and K. Tomishige, *ACS Catal.*, 2014, **4**, 2718-2726.

33. J. Wu, G. Gao, J. L. Li, P. Sun, X. D. Long and F. W. Li, *Appl. Catal. B-Environ.*, 2017, **203**, 227-236.

34. S. M. Rogers, C. R. A. Catlow, C. E. Chan-Thaw, A. Chutia, N. Jian, R. E. Palmer, M. Perdjon, A. Thetford, N. Dimitratos, A. Villa and P. P. Wells, *ACS Catal.*, 2017, **7**, 2266-2274.

35. Y. P. Su, C. Chen, X. G. Zhu, Y. Zhang, W. B. Gong, H. M. Zhang, H. J. Zhao and G. Z. Wang, *Dalton T.*, 2017, **46**, 6358-6365.

36. Z. R. Zhang, J. L. Song, Z. W. Jiang, Q. L. Meng, P. Zhang and B. X. Han, *Chemcatchem*, 2017, **9**, 2448-2452.

37. L. Prati and A. Villa, *Accounts Chem. Res.*, 2014, **47**, 855-863.

38. P. Paalanen, B. M. Weckhuysen and M. Sankar, *Catal. Sci. Technol.*, 2013, **3**, 2869-2880.

39. A. Villa, D. Wang, G. M. Veith, F. Vindigni and L. Prati, *Catal. Sci. Technol.*, 2013, **3**, 3036-3041.

40. F. Porta, L. Prati, M. Rossi, S. Coluccia and G. Martra, *Catal. Today*, 2000, **61**, 165-172.

41. J. K. Chinthaginjala, A. Villa, D. S. Su, B. L. Mojet and L. Lefferts, *Catal. Today*, 2012, **183**, 119-123.

42. X. Hu, S. Kadarwati, Y. Song and C. Z. Li, *RSC Adv.*, 2016, **6**, 4647-4656.

43. X. Chang, A. F. Liu, B. Cai, J. Y. Luo, H. Pan and Y. B. Huang, *Chemsuschem*, 2016, **9**, 3330-3337.

44. P. Panagiotopoulou, N. Martin and D. G. Vlachos, J. *Mol. Catal. A-Chem.*, 2014, **392**, 223-228.

45. P. Panagiotopoulou and D. G. Vlachos, *Appl. Catal. A-Gen.*, 2014, **480**, 17-24.

46. M. M. Villaverde, T. F. Garetto and A. J. Marchi, *Catal. Commun.*, 2015, **58**, 6-10.

47. A. N. Geraldes, D. F. da Silva, E. S. Pino, J. C. M. da Silva, R. F. B. de Souza, P. Hammer, E. V. Spinace, A. O. Neto, M. Linardi and M. C. dos Santos, *Electrochim. Acta*, 2013, **111**, 455-465.

48. G. Z. Chen, S. J. Wu, H. L. Liu, H. F. Jiang and Y. W. Li, *Green Chem.*, 2013, **15**, 230-235.

49. H. Q. Zhu, Z. F. Qin, W. J. Shan, W. J. Shen and J. G. Wang, *J. Catal.*, 2004, **225**, 267-277.

50. J. A. Lopez-Sanchez, N. Dimitratos, P. Miedziak, E. Ntainjua, J. K. Edwards, D. Morgan, A. F. Carley, R. Tiruvalam, C. J. Kiely and G. J. Hutchings, *Phys. Chem. Chem. Phys*., 2008, **10**, 1921-1930.

51. N. Dimitratos, J. A. Lopez-Sanchez, D. Morgan, A. F. Carley, R. Tiruvalam, C. J. Kiely, D. Bethell and G. J. Hutchings, *Phys. Chem. Chem. Phys.*, 2009, **11**, 5142-5153.

52. O. F. Aldosari, S. Iqbal, P. J. Miedziak, G. L. Brett, D. R. Jones, X. Liu, J. K. Edwards, D. J. Morgan, D. K. Knight and G. J. Hutchings, *Catal. Sci. Technol.*, 2016, **6**, 234-242.

53. N. Gyorffy and Z. Paal, J. Mol. Catal. A-Chem., 2008, **295**, 24-28.

54. Q. He, P. J. Miedziak, L. Kesavan, N. Dimitratos, M. Sankar, J. A. Lopez-Sanchez, M. M. Forde, J. K. Edwards, D. W. Knight, S. H. Taylor, C. J. Kiely and G. J. Hutchings, *Faraday Discuss.*, 2013.

55. A. Esfandiar, S. Ghasemi, A. Irajizad, O. Akhavan and M. R. Gholami, *Int. J. Hydrogen Energ.*, 2012, **37**, 15423-15432.

56. H. M. Qin, X. S. Qian, T. Meng, Y. Lin and Z. Ma, *Catalysts*, 2015, **5**, 606-633.

Figures and Tables:

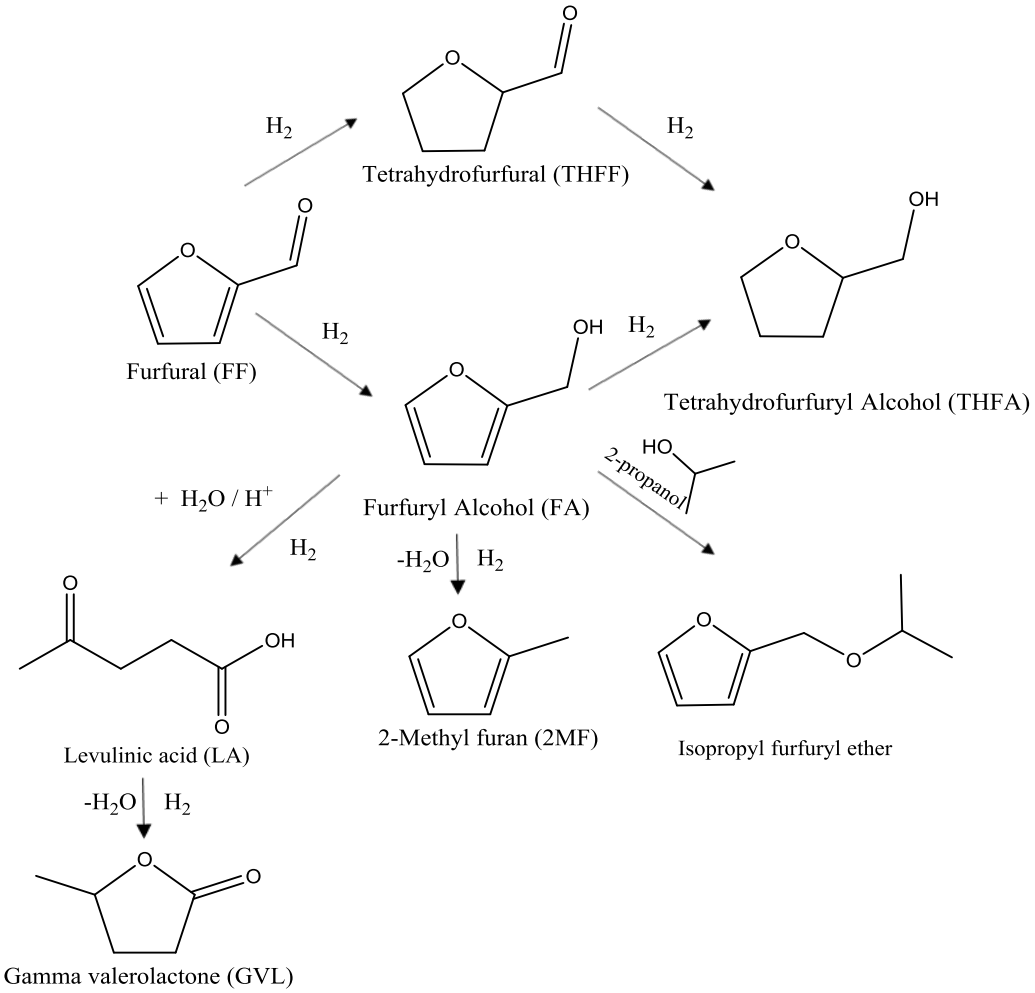

Figure 1. Schematic representation of the possible reaction pathways for the liquid phase hydrogenation of FF under mild conditions in the presence of supported Pd nanoparticles.

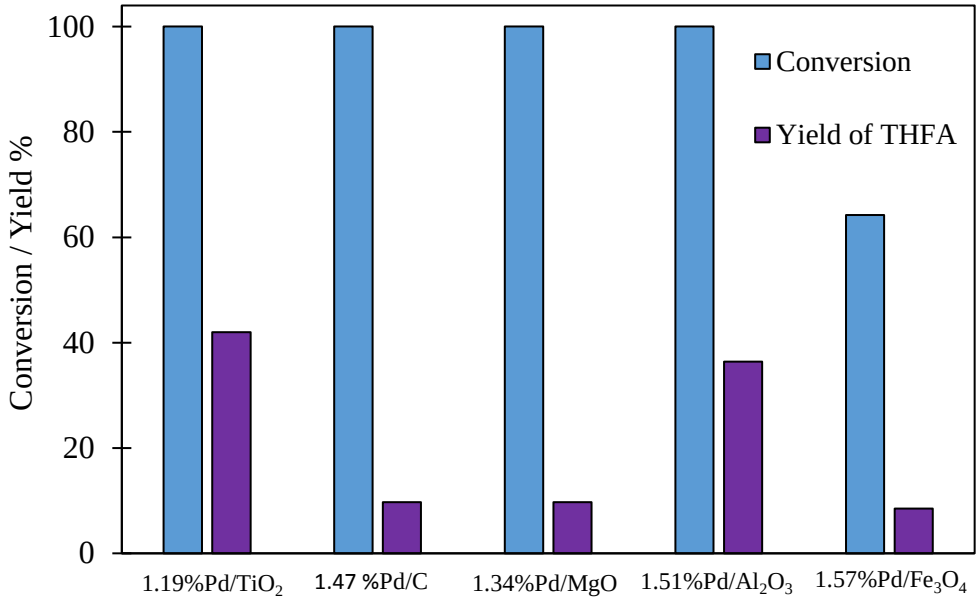

Figure 2. Effect of support on the yield of THFA produced in the liquid phase hydrogenation of FF. Reaction conditions: 0.3 M FF (15 ml), substrate/metal molar ratio = 500, 3 bar H_2, 30 °C, 180 min.

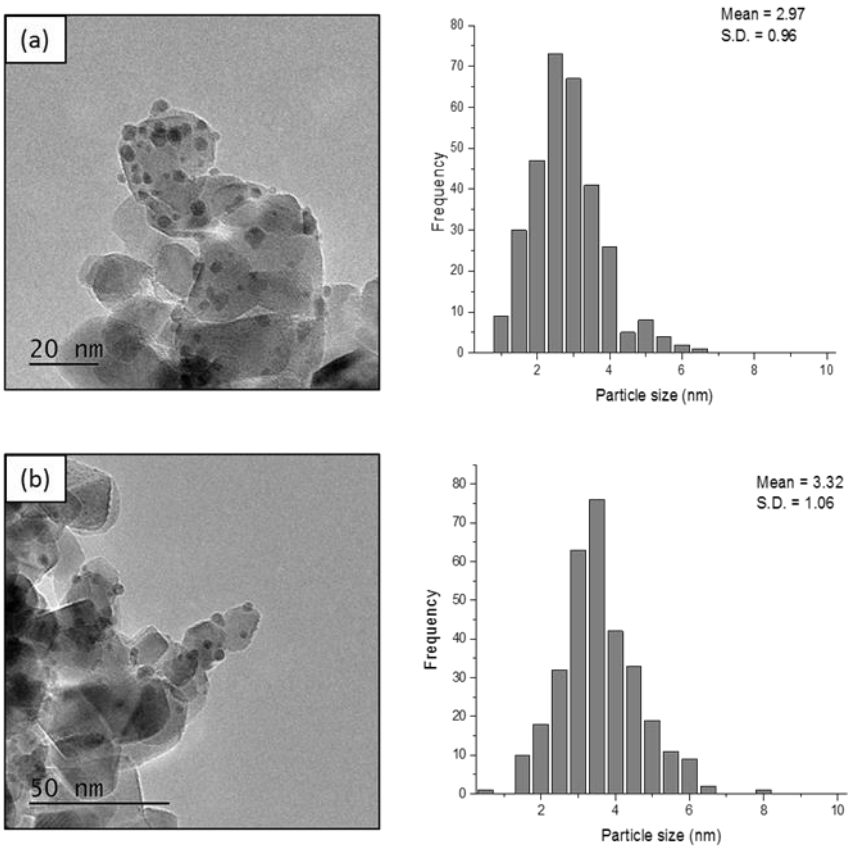

Figure 3. TEM images and corresponding particle size distribution for: (a) 0.57 % Pd/TiO_2 and (b) 1.19 % Pd/TiO_2.

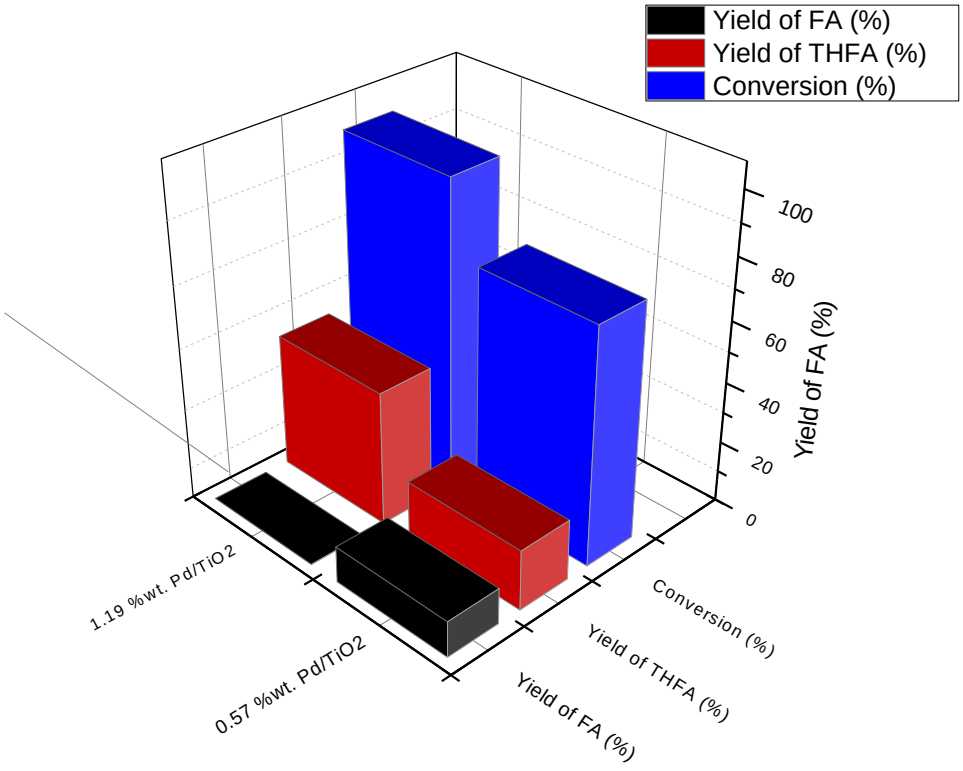

Figure 4. Graphical representation of the catalytic activity of Pd/TiO_2 prepared with different metal loading for liquid phase hydrogenation of FF. Reaction conditions: 0.3 M FF (15 ml), substrate/metal molar ratio = 500, 3 bar H_2, 30 °C, 120 min.

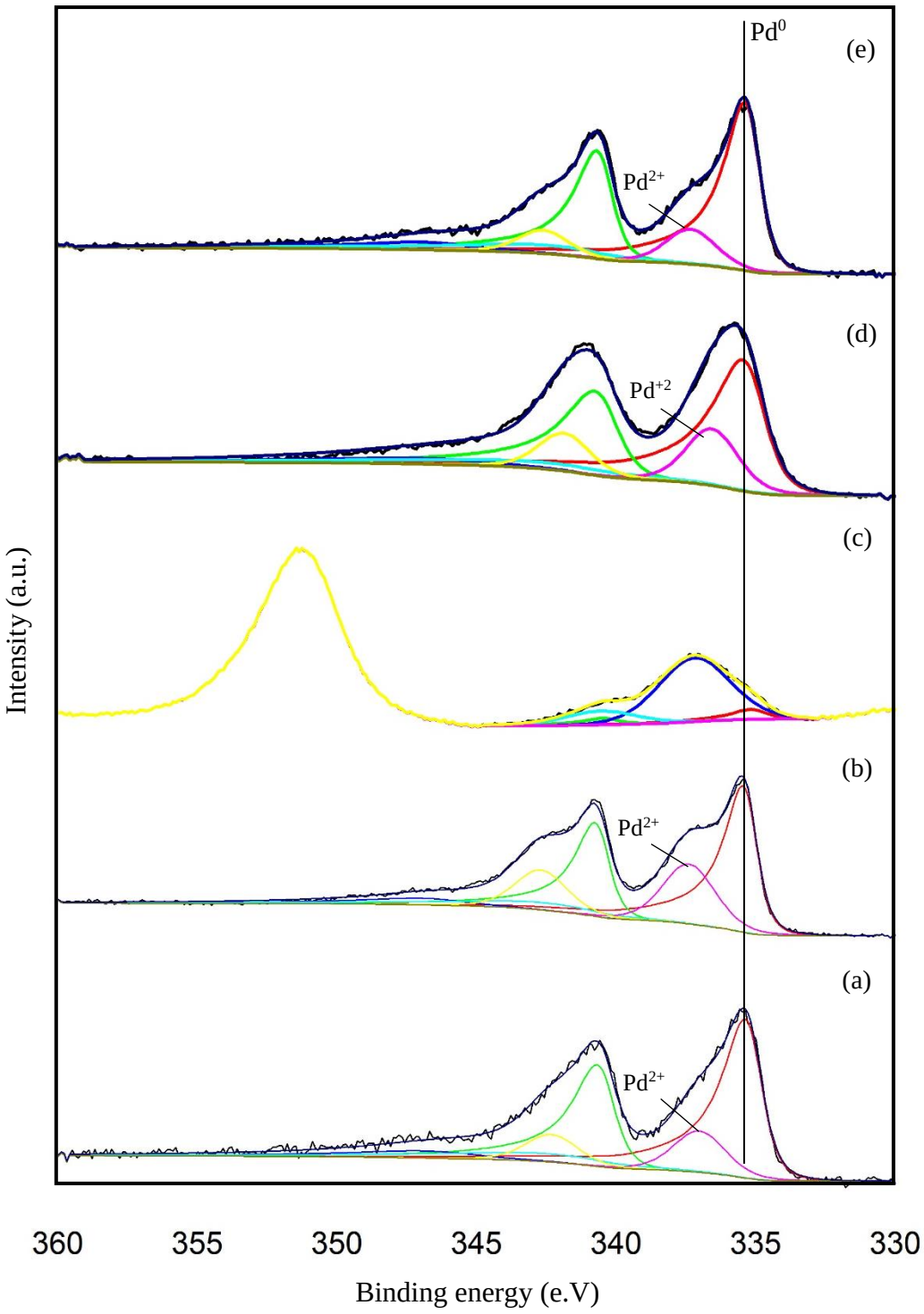

Figure 5. Pd 3d core-level XPS spectra of the supported Pd catalysts (a)1.19 % Pd/TiO_2, (b) 1.47 % Pd/C, (c) 1.34 % Pd/MgO, (d) 1.51 % Pd/Al_2O_3 and (e)1.57 % Fe_3O_4.

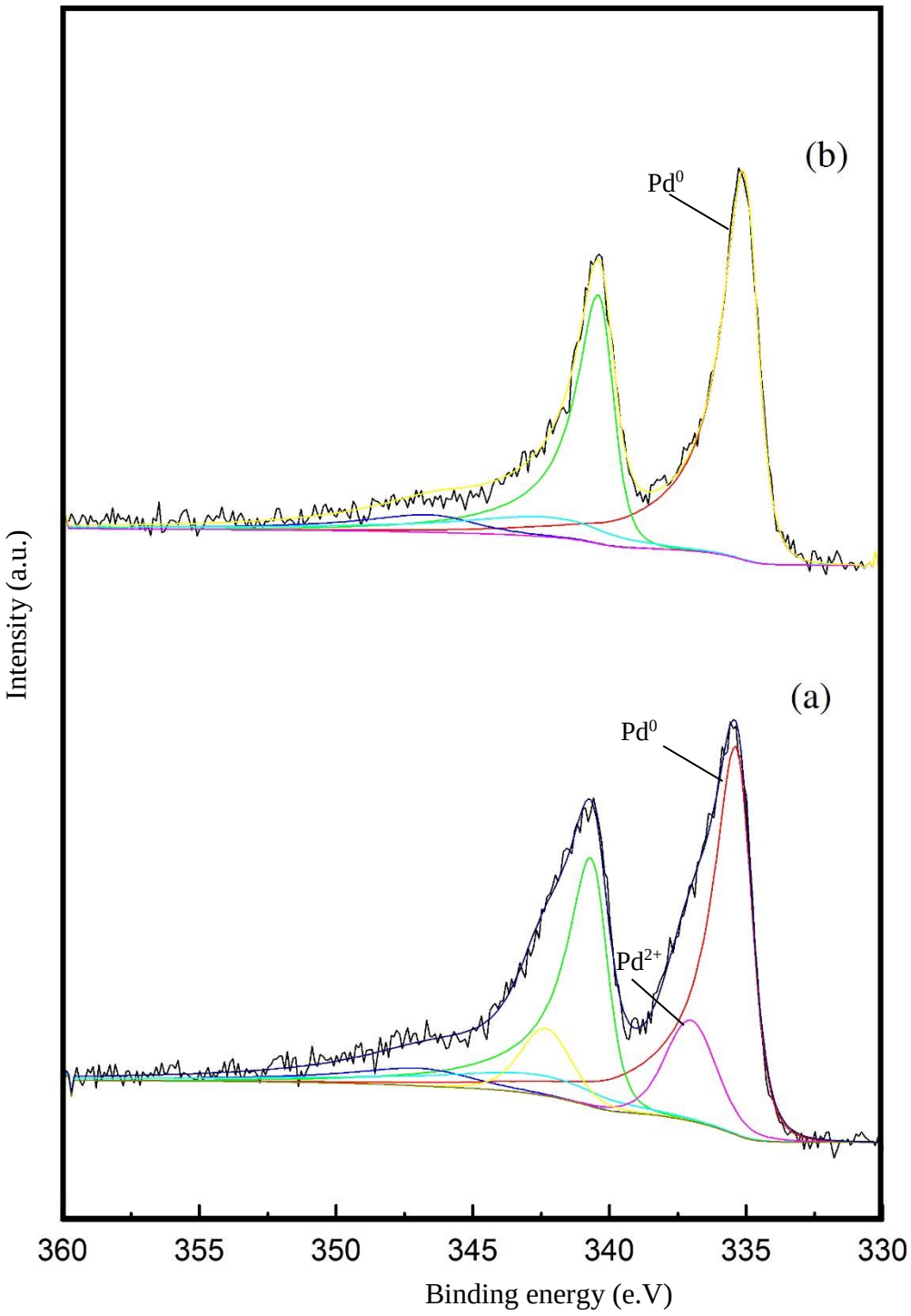

Figure 6. Pd 3d core-level XPS spectra of the 1.19 % Pd/TiO_2 catalyst (a) Fresh sample and (b) used sample after the liquid phase dehydrogenation of FF.

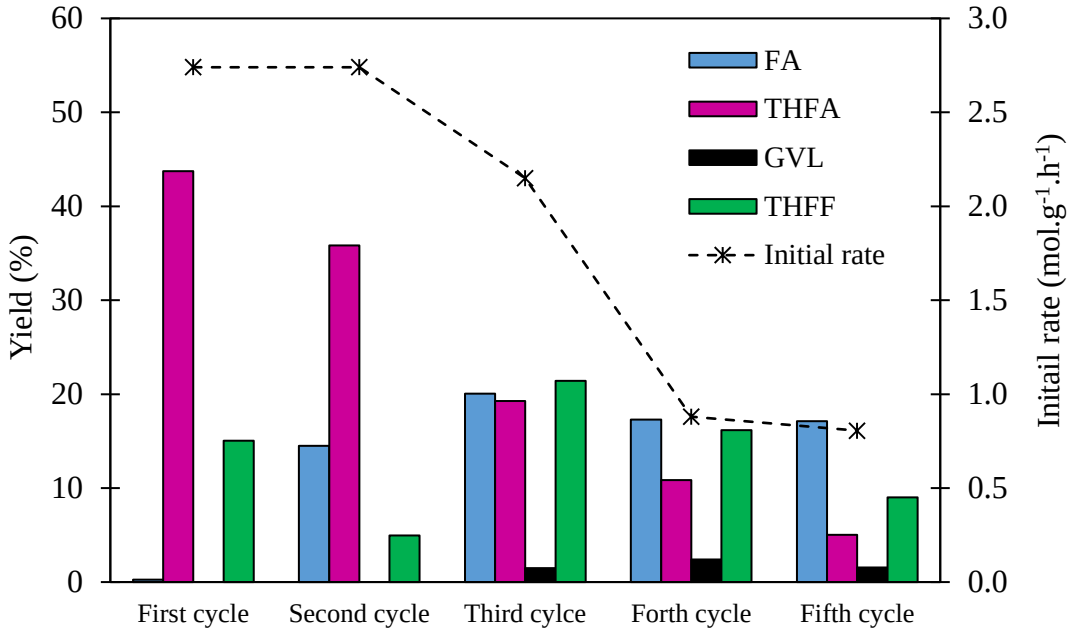

Figure 7. Reusability of the 1.19 % Pd/TiO_2 in liquid phase hydrogenation of furfural. Reaction conditions: 0.3 M FF (15 ml), substrate/metal molar ratio = 500, 3 bar H_2, 30 °C, reaction time 120 min. Initial rate calculated after 30 min.

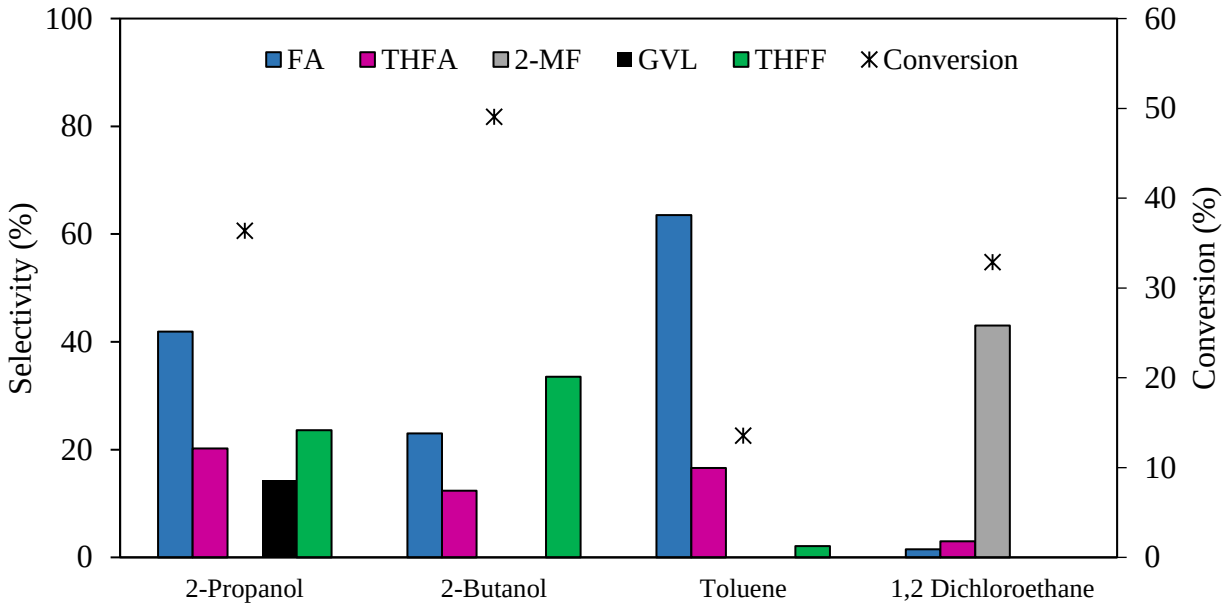

Figure 8. Effect of solvent on the catalysed hydrogenation of FF over a 1.19 % Pd/TiO_2. Reaction Conditions: 0.3 M FF (15 ml), substrate/metal molar ratio = 500, 3 bar H_2, 30 °C, reaction time 30 min.

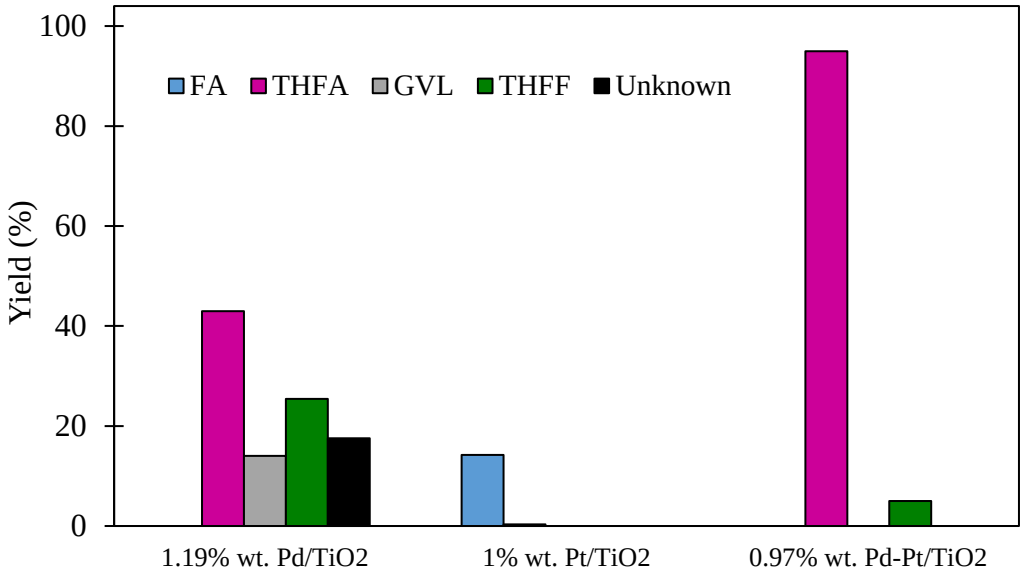

Figure 9. A Comparison of product yields for the catalysed hydrogenation of FF using monometallic Pd/TiO_2 and Pt/TiO_2 catalysts with bimetallic $PdPt/TiO_2$. Reaction Conditions: 0.3 M FF (15 ml), substrate/metal molar ratio = 500, 3 bar H_2, 30 °C.

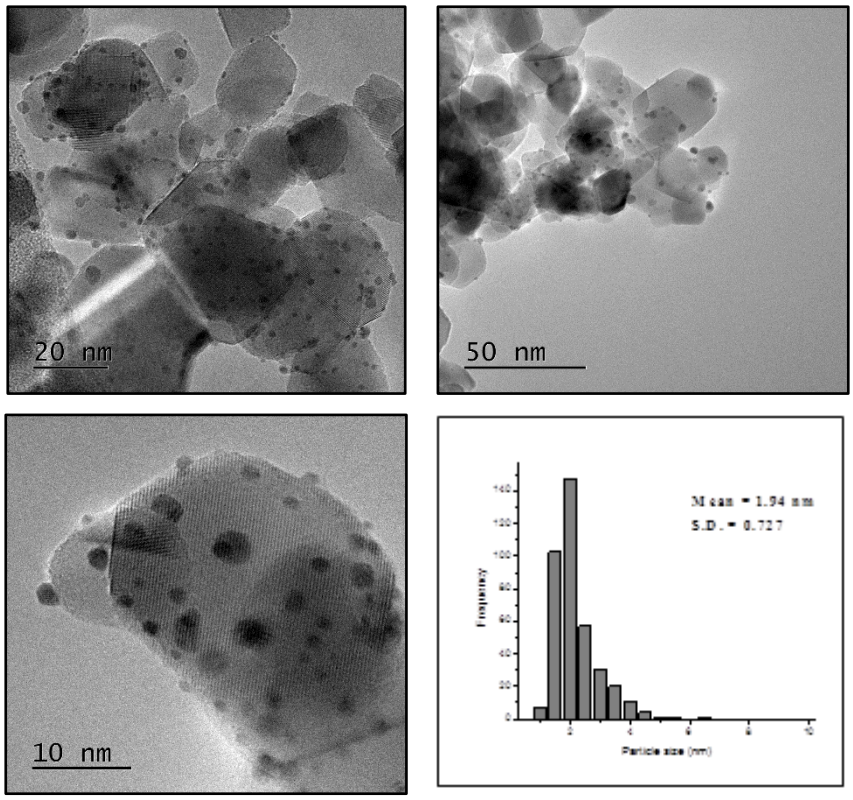

Binding energy (e.V)

Figure 10. TEM images and corresponding particle size distribution for 0.97 % PdPt/TiO_2.

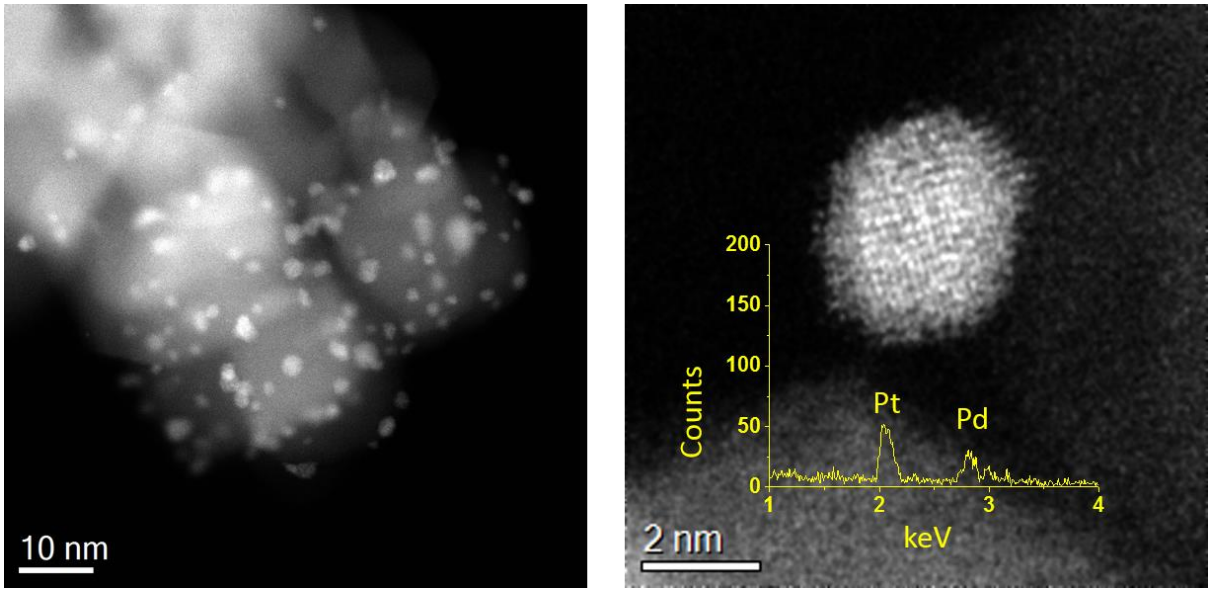

Figure 11. Scanning Transmission Electron Microscopy (STEM) characterization of the Pd-Pt/TiO_2 catalyst. (a) relatively lower magnification and (b) higher magnification image of the nanoparticles. From the HAADF Z-contrast imaging and the X-ray Energy Dispersive Spectrum (X-EDS) (image inlet) taken from the individual particle, the formation of random Pd-Pt nanoalloy can be confirmed.

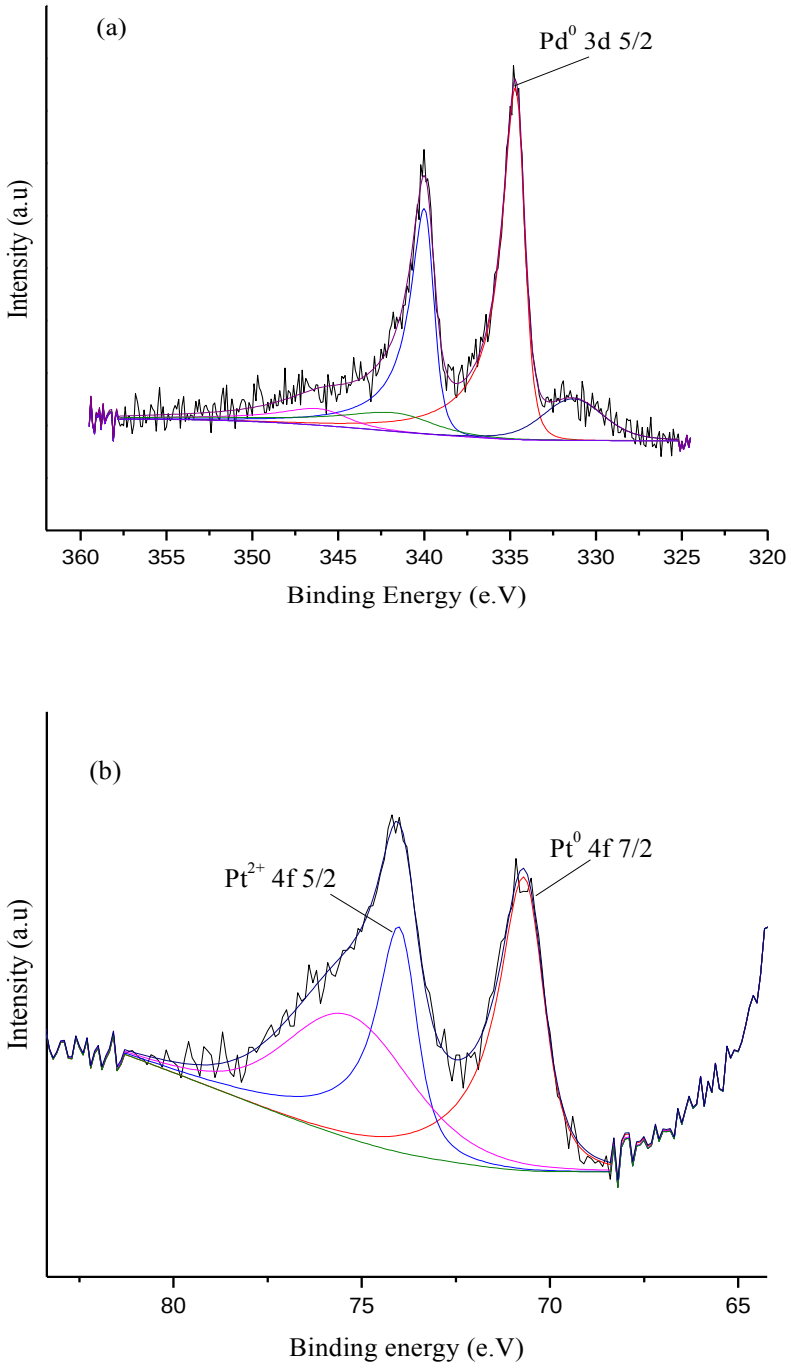

Figure 12. XPS peak deconvolution of (a) Pd and (b) Pt in 0.97 % Pd-Pt/TiO_2 catalyst.

Table 1. Reaction systems reported in the literature for the total hydrogenation of FF to FA.

Catalyst	Solvent	Moles of FF	Temp	H_2 Pressure	Catalyst Mass	Time	THFA Yield	Primary Author
		[mmol]	[ºC]	[bar]	[g]	[h]	[%]	
RuO_2	MeOH	270.61	120	40	2	1	76	Merat[29]
Ni-Pd/SiO_2	H_2O	5	40	80	0.1	2	96	Nakagawa[30]
Raney Ni-$Al(OH)_3$	2-Propanol	1.04	110	30	0.05	1.25	> 99	Rodiansono[31]
Pd-Ir/SiO_2	H_2O	5	2	80	0.15	6	94	Nakagawa[32]
CuNi/MgAlOx	Ethanol	5	150	40	0.05	3	95	Gao[33]
Pd/C	2-Propanol	4.5	25	5	0.096	5	45	Rogers[34]
Ni/C	2-Propanol	0.31	120	30	0.03	2	100	Su[35]
Ru-C/TiO_2	1-Butanol	1	80	40	0.03	5	100	Zhang[36]

Table 2. The selective hydrogenation of FF over a series of Pd supported catalysts. Reaction Conditions: 0.3 M FF (15 ml), solvent: 2-propanol, catalyst (0.1 g), 30 ºC, 3 bar H_2.

Catalysts	Metal* loading	Reaction time	Conversion	Selectivity [%]						Initial rate
	[%]	[Min]	[%]	FA	THFA	2-MF	GVL	THFF	Unknown	mol g^{-1} h^{-1}
Pd/TiO_2	1.19	30	36.4	41.9	20.2	0.0	14.3	23.6	0.0	2.75
		90	98.6	4.1	33.9	0.0	12.7	26.2	23.1	
		180	100.0	0.0	42.0	0.0	14.0	25.4	18.5	
Pd/C	1.47	30	85.2	35.3	4.2	6.1	10.6	4.5	39.2	5.21
		90	100.0	6.2	9.3	22.5	10.5	4.6	47.0	
		180	100.0	0.5	9.7	15.9	8.7	4.0	61.2	
Pd/MgO	1.34	30	43.0	8.5	2.3	0.0	0.0	89.1	0.0	2.89
		90	99.2	3.1	7.2	0.0	0.0	89.7	0.0	
		180	100.0	0.1	9.7	0.0	0.0	80.0	10.2	
Pd/Al_2O_3	1.51	30	53.5	14.4	5.8	0.0	0.0	6.6	73.3	3.19
		90	100.0	3.0	33.3	0.0	11.0	43.1	9.5	
		180	100.0	0.1	36.4	0.0	11.5	42.4	9.6	
Pd/Fe_2O_3	1.57	30	7.2	32.5	13.3	0.0	0.0	53.4	0.8	0.41
		90	33.2	10.2	8.1	0.0	1.4	30.1	50.2	
		180	64.2	6.4	8.5	0.0	1.3	25.2	58.6	

* Pd weight loading determined by MP-AES

Table 3. Effect of temperature on the catalysed hydrogenation of FF over a 1.19 % Pd/TiO_2 catalyst. Reaction Conditions: 0.3 M FF (15 ml), substrate/metal molar ratio = 500, 3 bar H_2.

Temperature	Reaction time	Conversion	Selectivity [%]					Initial rate
C°	[Min]	[%]	FA	THFA	GVL	THFF	Unknown	mol g^{-1} h^{-1}
30	30	36.3	41.8	20.2	14.3	23.6	0.0	2.75
	120	100.0	0.3	43.7	15.0	29.9	11.0	
50	30	44.7	31.5	12.1	9.1	13.8	33.4	3.39
	120	100.00	10.7	27.8	14.2	10.9	36.4	
60	30	56.4	19.9	3.5	3.1	7.9	65.5	4.27
	120	73.3	38.1	11.0	8.1	12.5	30.3	

Table 4. Effect of hydrogen pressure on the catalysed hydrogenation of FF over a 1.19 % Pd/TiO_2 catalyst. Reaction Conditions: 0.3 M FF (15 ml), substrate/metal molar ratio = 500, 30°C.

Hydrogen Pressure	Reaction time	Conversion	Selectivity [%]						Initial rate
	[Min]	[%]	FA	THFA	2-MF	GVL	THFF	Unknown	mol g^{-1} h^{-1}
1.00	30.00	21.56	43.38	11.22	0.00	5.57	22.00	17.83	1.63
	120.00	62.60	21.88	18.26	0.00	10.31	19.54	30.01	
2.00	30.00	22.98	50.77	12.21	0.00	8.71	18.09	10.21	1.74
	120.00	96.09	9.89	27.94	0.00	16.12	15.11	30.93	
3.00	30.00	36.36	41.87	20.21	0.00	14.31	23.57	0.04	2.75
	120.00	100.00	0.28	43.74	0.00	15.04	29.99	10.95	

Table 5. A Comparison of catalytic performance of monometallic Pd/TiO_2 and Pt/TiO_2 catalysts with a bimetallic $PdPt/TiO_2$ for the catalysed hydrogenation of FF. Reaction Conditions: 0.3 M FF (15 ml), substrate/metal molar ratio = 500, 3 bar H_2, 30 °C

Catalysts	Metal content* [wt %]		Reaction time	Conversion	Selectivity [%]						Initial rate
	Pd	Pt	[Min]	[%]	FA	THFA	2-MF	GVL	THFF	Unknown	mol g^{-1} h^{-1}
Pd/TiO_2	1.19	-	30	36.4	41.9	20.2	0.0	14.3	23.6	0.00	2.75
			120	100.0	0.3	43.7	0.0	15.0	30.0	10.95	
			240	100.0	0.0	42.0	0.0	14.0	25.4	18.52	
Pt/TiO_2	-	1	30	7.0	100.0	0.0	0.0	0.0	0.0	0.00	0.66
			120	13.2	98.2	1.8	0.0	0.0	0.0	0.00	
			240	14.5	98.1	2.3	0.0	0.0	0.0	0.00	
$Pd\text{-}Pt/TiO_2$	0.47	0.49	30	52.9	65.7	14.7	0.0	0.0	0.0	19.62	11.03
			120	96.8	71.3	27.3	0.0	0.0	1.5	0.00	
			240	100.0	0.0	95.0	0.0	0.0	5.0	0.00	

*Metal content was determined by MP-AES